





Large-scale dynamics moderate impact-relevant changes to organised convective storms

Steven C. Chan ^{1,2✉}, Elizabeth J. Kendon ^{2,3}, Hayley J. Fowler¹, Abdullah Kahraman ^{1,2}, Julia Crook⁴, Nikolina Ban^{5,7} & Andreas F. Prein ⁶

Larger organised convective storms (mesoscale-convective systems) can lead to major flood events in Europe. Here we assess end-of-century changes to their characteristics in two convection-permitting climate simulations from the UK Met Office and ETH-Zürich that both use the high Representative Concentration Pathway 8.5 scenario but different approaches to represent atmospheric changes with global warming and different models. The UK Met Office projections indicate more frequent, smaller, and slower-moving storms, while ETH-Zürich projections show fewer, larger, and faster-moving storms. However, both simulations show increases to peak precipitation intensity, total precipitation volume, and temporal clustering, suggesting increasing risks from mesoscale-convective systems in the future. Importantly, the largest storms that pose increased flood risks are projected to increase in frequency and intensity. These results highlight that understanding large-scale dynamical drivers as well as the thermodynamical response of storms is essential for accurate projections of changes to storm hazards, needed for future climate adaptation.

¹School of Engineering, Newcastle University, Newcastle upon Tyne, UK. ²Met Office Hadley Centre, Exeter, UK. ³University of Bristol, Bristol, UK. ⁴University of Leeds, Leeds, UK. ⁵ETH-Zürich, Zürich, Switzerland. ⁶National Center for Atmospheric Research, Boulder, CO, USA. ⁷Present address: Universität Innsbruck, Innsbruck, Austria. ✉email: steven.chan@newcastle.ac.uk

The hazards posed by heavy precipitation events increase with higher intensity and longer-duration storms. Flooding is most likely when prolonged intense precipitation falls on the same area¹. In Europe, such multi-hour intense precipitation events often manifest in the form of mesoscale-convective systems (MCSs^{2,3}; large areas of convective precipitation, defined here as contiguous precipitating areas exceeding 1000+ km² with maximum precipitation exceeding 20 mm/h averaged over a 144 km² grid box). MCSs are important contributors to extreme precipitation during the warm season (summer and autumn) in Europe⁴. Elsewhere, MCSs can contribute more than half of the annual total precipitation, like over the Great Plains and the La Plata Basin^{3,5}.

MCSs have a large spatial extent, which can lead to high precipitation totals over a catchment. While most MCSs last for only a few hours, some last for more than 18 h⁶. MCSs may appear quasi-linear (e.g. squall lines) or quasi-circular. While we focus on the precipitation from MCSs, they cause other weather hazards such as intense wind gusts, tornadoes, hail, and lightning. Over Europe, MCSs have caused substantial casualties and damages. A selection of events is shown in Table 1 involving different MCS hazards, but the focus in this paper is on extreme precipitation.

The large-area and longevity of MCSs are tied to their interaction with the large-scale synoptic dynamic conditions at scales exceeding 1000 km. Large-scale winds control the vertical wind shear, which are crucial for MCS upscale growth and persistence. Weakly-sheared convective environments may lead to poorer-organised and typically slower-moving storms, but slow-moving storms cause longer precipitation durations at a given location and hence higher local precipitation accumulations¹; this is in contrast with bigger and long-lived MCSs that have higher lifetime total precipitation volume, spreading over larger areas. Total precipitation volume is also closely linked to precipitation rate, which is controlled by the thermodynamics of the storm environment, fed by synoptic/mesoscale structures like low-level jets⁷. MCS area, lifetime, movement speed, storm precipitation rate and total volume can all be diagnosed by methods that track individual storms⁸.

Proper simulation of MCSs requires a model able to represent the underlying mesoscale dynamics. Some current-generation climate and forecast models have grid box sizes of ~1 km which enables the (deep) cumulus parameterisation to be switched off (convection-permitting models, hereby CPMs). CPMs are capable of partially-resolving convection and reduce some biases typically associated with the use of cumulus parameterisation^{9–15}. CPMs have been shown to simulate realistic frequency and tracks of North American MCSs¹⁶ and more realistic MCS properties over Africa than lower-resolution parameterised-convection models¹⁷. CPMs have also been shown to reasonably represent key observed

characteristics of intense precipitation events over the north-west Mediterranean, while underestimating the highest precipitation intensities¹⁴.

This study uses a series of the UK Met Office (UKMO) Unified Model and ETH-Zürich (ETHZ) COSMO Europe-wide 2.2 km CPM simulations^{11,18–20}. These include ERA-Interim-driven hindcasts (1999–2008; UKMO:CPMU_H, ETHZ:CPMC_H) for both CPMs. However, the CPMs use different approaches to represent atmospheric changes due to global warming. The UKMO downscales a free-running global climate model for the present-day (driven by 1998–2007 sea surface temperatures; CPMU_P) and for future-climate (same SST superposed with changes at the end of the century, 10 years long; CPMU_F), while ETHZ uses a “pseudo-global warming” (PGW) simulation representing future-climate at the end of the century (10 years long; CPMC_{PGW}). The PGW approach²¹ involves modifying the ERA-Interim boundary conditions used for the hindcast to capture the mean warming signal and associated changes in moisture and large-scale circulation, whilst the sequence of weather systems is unchanged. This allows the thermodynamic component of the future change²² to be robustly captured, with reduced influence from natural variability. Previous work over the US, using a PGW approach, showed increases in the frequency and precipitation volume of MCSs with global warming²³. However, the PGW approach has limitations in representing variance changes driven by global warming^{21,24}, which can be a critical control on MCS characteristics such as duration and area¹; i.e., PGW cannot represent changes to the sequencing and timing of weather events and intra-seasonal/inter-annual modes such as the North Atlantic Oscillation (NAO). On the other hand, with the standard GCM downscaling approach, we assume that these changes are well represented by the driving GCM, noting that state-of-the-art GCMs still have significant biases in both the variance and the mean climate^{25,26}.

Here, to the best of our knowledge for the first time, we compare changes to MCSs in a full dynamical GCM-downscaled simulation (CPMU_F) to those from a PGW simulation (CPMC_{PGW}) at the convection-permitting scale for the late-C21 under the Representative Concentration Pathway (RCP) 8.5²⁷, using two different convection-permitting regional climate models. The influence of dynamical changes in circulation patterns on MCSs has not previously been considered at convection-permitting scales. Using a single-GCM downscaling approach, it is not possible to represent the uncertainty in projected changes, e.g. Coupled Model Intercomparison Project (CMIP) projections show good agreement in the reduction of summer synoptic variability over Europe but consensus is low for mean troposphere wind changes^{28,29}. This uncertainty to mean dynamical changes is often used as a justification for the PGW approach with the drawback of not representing changes in intra-seasonal variability.

Most results are based on a Europe-wide analysis, but we do select three sub-domains for more detailed analysis. They are the British Isles, Germany, and “Alpine” region. They are described in the Methods and Supplementary Fig. 1.

We employ an automatic method for MCS detection and tracking^{8,17}. Previous work applying a severe storm ingredients-based approach¹ to the CPMU_F simulation indicated a future increase in slow-moving storms with the potential for high precipitation accumulations, attributing that to weakening of upper tropospheric winds³⁰. Here, to the best of our knowledge for the first time, we provide insight into the role of large-scale circulation changes in driving changes to MCSs. We explore changes to MCS sequencing across Europe, as well as characteristics of MCSs.

Table 1 Examples of notable European extreme weather events that could be attributable to MCSs and organised convective extremes.

Notable recent European convective events

Event	Hazard	Fatalities	Damages
Southern France 2002-09-08/09 ⁷³	Heavy precipitation Flash flooding	24	€ 1200 million
Germany and Belgium 2014-06-09 ⁷⁴	Wind Hail	6	€ 650 million
Czech Republic 2021-06-24 ⁷⁵	Tornadoes	5	12,000+ million CZK (≈€450+ million)

Casualties and estimated damage figures included.

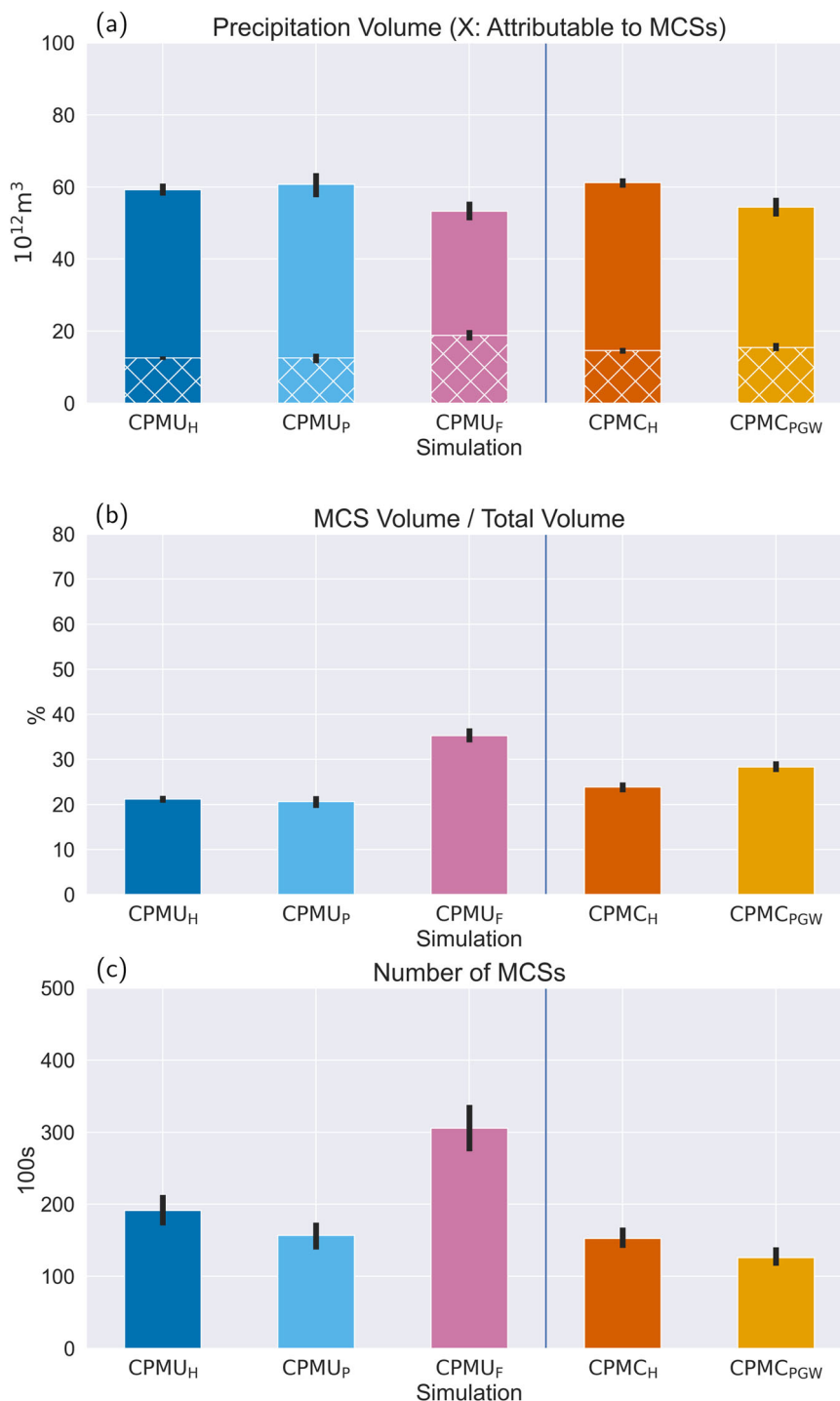


Fig. 1 Ten-year total precipitation volume attributable to MCSs across Europe and their counts. Here we show **a** total precipitation volume calculated from daily mean precipitation plus the part that is attributable to MCS (cross-hashed area), **b** the percentage contribution from MCSs, and **c** the number of MCSs. Black lines are the 95% CIs, estimated by year-block bootstrapping 1000 times.

Results and discussion

We first examine the percentage of total precipitation contributed by MCSs and the number of MCSs in the present-day and future simulations. Figure 1 indicates that MCSs currently cause $\approx 20\text{--}25\%$ of the total precipitation ($\approx 10\text{--}15$ trillion m^3), with agreement across CPMs. In a future warmer climate, both CPMs project a decrease in mean precipitation of $\approx 12\%$, largely due to warm season decreases (Supplementary Note 1) but a substantial increase in the contribution from MCSs. The CPMU_F simulation projects almost a doubling of MCS contribution (from

$20.6\% \rightarrow 35.3\%$); a smaller increase is projected from CPMC_{PGW} (from $23.9\% \rightarrow 28.3\%$), with both increases significant compared to year-to-year variability.

Despite this agreement, the CPMs project different changes to the frequency of MCSs: CPMU_F shows a near doubling, but CPMC_{PGW} shows a $\approx 18\%$ decline. This might be related to different spatial patterns in present-day MCS frequencies (Fig. 2a–c). Both models agree on a northward decrease in MCS frequencies consistent with observations^{5,31,32}, but CPMU_H and CPMU_P favour MCSs over the Western Mediterranean while

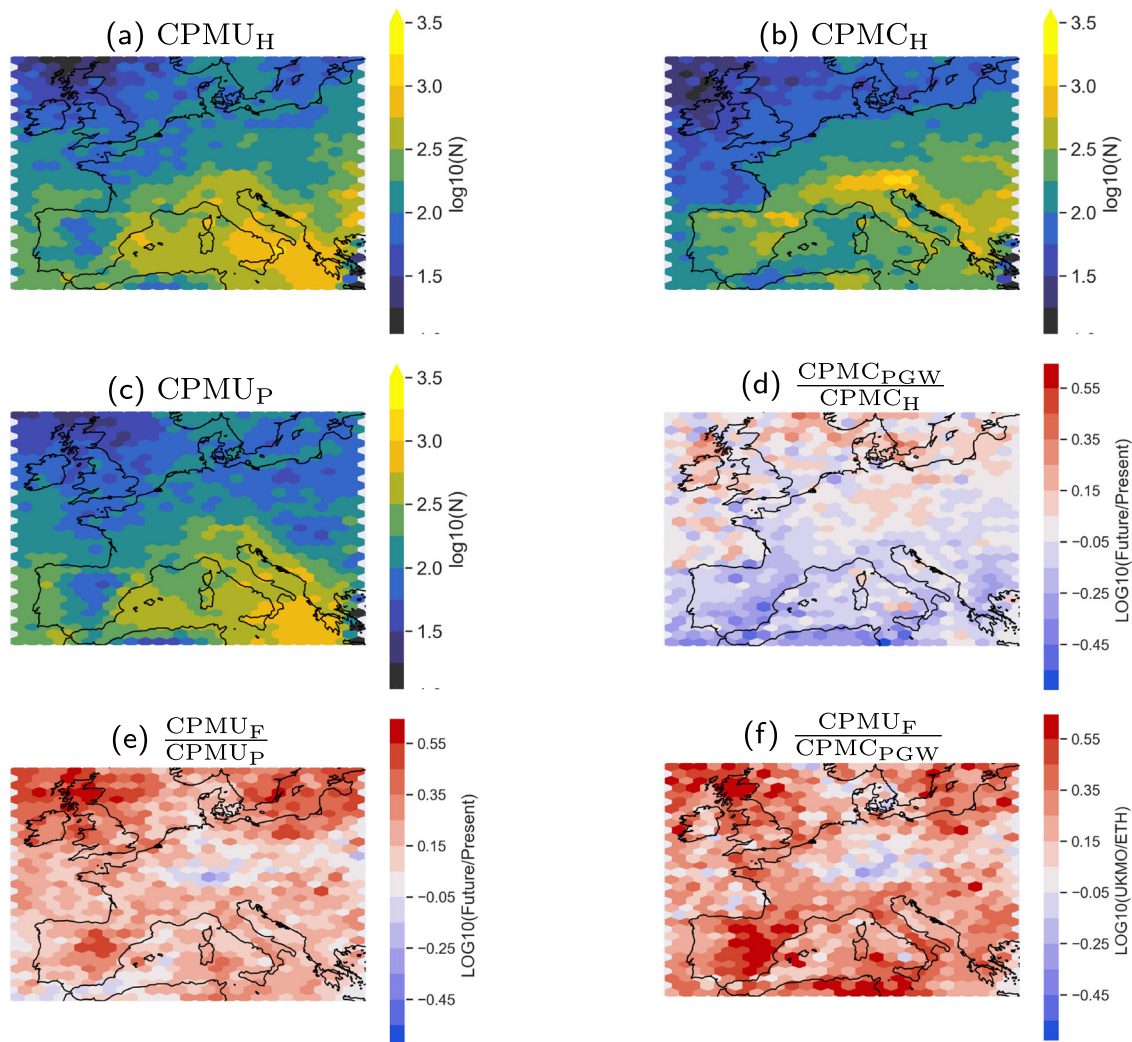


Fig. 2 Spatial frequency of MCSs across Europe. Shown are logarithm counts ($\log N$) for **a, b** UKMO and ETH hindcast, and **c** UKMO present-climate simulation in hexagon bins⁷⁶. Future changes as logarithm ratios for **d** ETH (PGW/hindcast) and **e** UKMO (future/present) and **f** ratio of UKMO to ETH future changes.

CPMC_H favours storms over land. We explore this further in Supplementary Note 2 by comparing our results with recent satellite analysis estimates. The future changes to MCS frequency do not show any clear spatial pattern (Fig. 2d, e). The increase (decrease) projected by CPMU_F (CPMC_{PGW}) simulations is relatively consistent across the entire domain with better agreement over Central Europe (decreases for both CPMs) (panel f).

We now move on to examine the present-day simulation and changes to a number of key storm statistics—precipitation volume, maximum and average intensity, MCS movement speed, maximum area, and storm lifetime (Figs. 3 and 4). The maximum intensity, area, and movement speed of an MCS determines local precipitation accumulation and is hence important to localised flash flooding^{30,33}. MCS lifetime precipitation volume is important for accumulations over larger catchments and hence wider flood impacts. We also examine temporal clustering across Europe, as well as national-scale regions. Temporal clustering is an important control on antecedent moisture conditions and hence the probability of flooding, but also to compounding impacts through increased vulnerability.

Many studies have reported increases in the intensity of extreme precipitation with warming^{22,34–36}. Here we use an intensity threshold (20 mm h^{-1}) to track MCSs (Fig. 3a). The 95th percentile peak intensity of those MCSs is $\approx 45 \text{ mm h}^{-1}$ for

both CPMs present-day simulations. We find that both models show an overall intensification, with CPMC_{PGW} showing a lower intensification of the 95th percentile of $\approx 15\%$, compared to a 24% increase for CPMU_F. Although CPMU_F shows a significant increase in MCS frequency at all intensities (Fig. 3b), we find the largest increases in absolute counts for the highest peak intensity events (e.g. about a tripling for $40\text{--}45 \text{ mm h}^{-1}$). Importantly, we find MCSs in the future simulation with unprecedented ($70+ \text{ mm h}^{-1}$) peak hourly intensities. For CPMC_{PGW}, we find the same frequency increase for storms with the highest intensities ($45+ \text{ mm h}^{-1}$), but a projected decrease in the overall number of MCSs. Consistent with increasing peak intensities, both CPMs project an increase to MCS area-averaged intensity (Fig. 3c, d). Higher increases are found for CPMU_F, with 95th percentile area-averaged precipitation intensity increased by 1.7 mm h^{-1} (+22%) respectively, relative to smaller 0.8 mm h^{-1} (+10%) increases from the PGW-CPM simulations.

We now analyse precipitation volume from individual MCSs (Fig. 3e, with the vertical line indicating the 95th percentile). CPMU_F shows a large increase in low volume (Fig. 3f; PrVol $\leq 10^8 \text{ m}^3$) storms, with the 95th percentile ($10^{9.4} \approx 2.5 \times 10^9 \text{ m}^3$) of the future-climate simulation less than the present-day simulation. This means a future CPMU_F MCS typically produces a lower volume of precipitation over its lifetime even though there is a

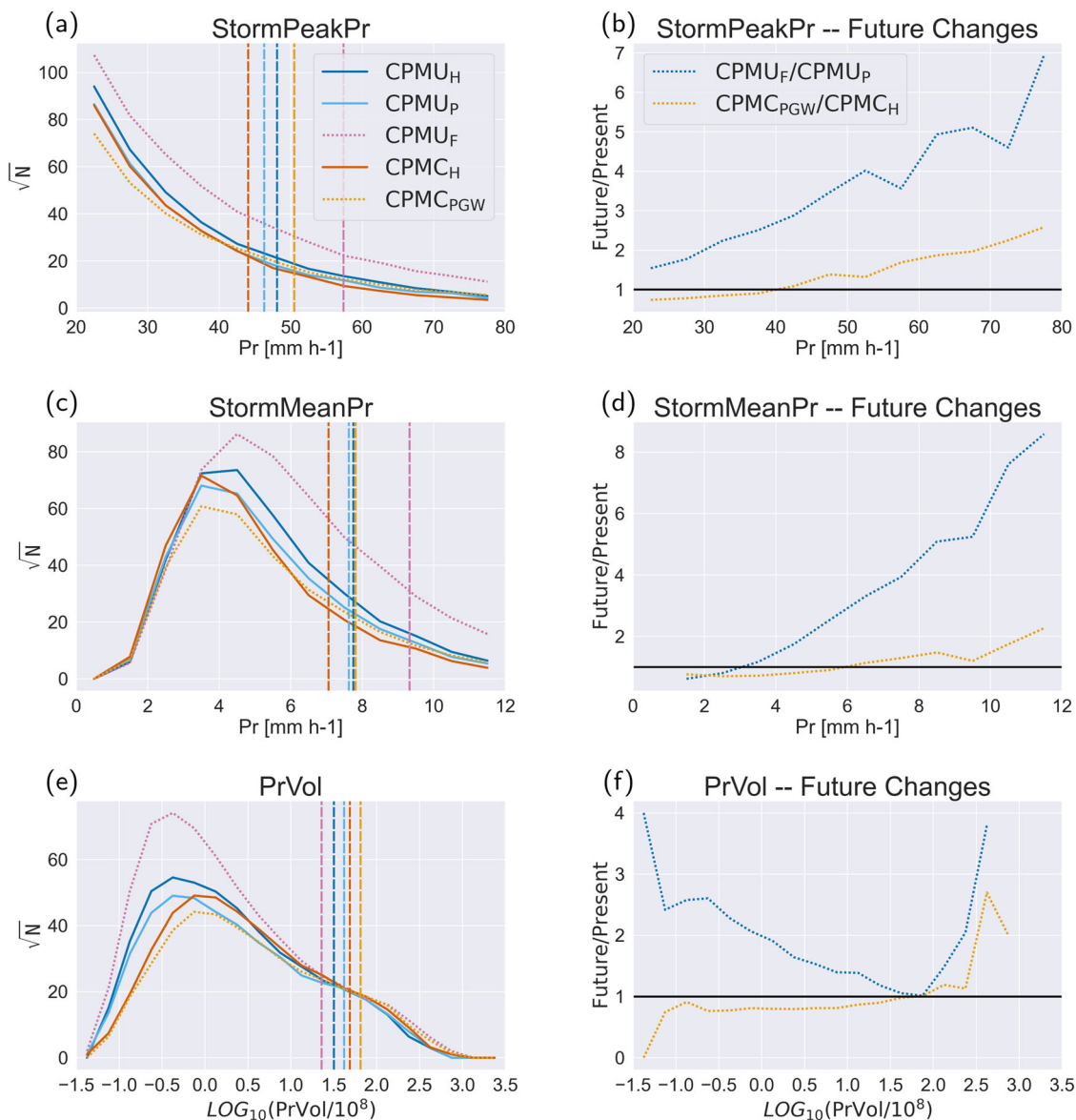


Fig. 3 Histograms of various storm properties and their future changes. Square roots of counts on **a, c, e**: CPMU_H (cyan), CPMU_P (dark blue), CPMU_F (purple) CPMC_H (orange), and CPMC_{PGW} (red). Future changes as ratios on **b, d, f**: UKMO (purple), ETHZ (brown). The properties are **a, b** MCS peak intensity (StormPeakPr), **c, d** average precipitation rate per model grid point over the MCS (StormMeanPr), and **e, f** precipitation volume (PrVol). Vertical lines on **a, c, e** indicate the 95th percentile for each model simulation. For **e**, the percentage PrVol contribution from all storms exceeding PrVol 80th percentile are: 87% CPMU_H, 88% CPMU_P, 90% CPMU_F, 86% CPMC_H, and 87% CPMC_{PGW}.

much higher frequency of these MCSs (Fig. 1). In contrast for CPMC_{PGW}, there is a decrease of MCSs with low volumes, but frequency changes for higher volume storms are small, resulting in an increase to the 95th percentile MCS volume. Both CPMs therefore show a future increase in the total precipitation resulting from MCSs, but changes in the underlying characteristics of the MCS population are quite different.

Importantly, we find that both modelling approaches indicate future increases to the absolute number of high-volume, and thus impactful, MCSs. Both UM and COSMO present-day 95th percentiles for precipitation volume per MCS (Fig. 3e) are just above 1.5 (precisely, $10^{1.5} \times 10^8 \approx 3$ billion m³). Future total precipitation volume above 1.5 are increased by about 52% and 17% for CPMU_F and CPMC_{PGW} respectively. The top 20% wettest MCSs in all simulations contribute close to 85–90% of the total annual precipitation from all MCSs, following the 80–20 Pareto principle, and hence explains agreement with satellite analysis estimates

since they are biased in favour of larger-area MCSs. Weaker MCSs, despite being more numerous, have a smaller contribution. Hence, future changes to total MCS precipitation volume are dominated by changes at the tail of the distribution: for both CPMU_F and CPMC_{PGW}, there are increases of total precipitation volume attributable to the top 20% wettest MCSs (UKMO: 88% ↗ 90%; ETHZ: 86% ↗ 87%).

We now move on to examine the temporal variability of MCSs. We might expect MCSs to naturally cluster in time when conditions are favourable, and this is likely different in the future climate³⁷. Temporal clustering on sub-seasonal timescales magnifies the impact of MCSs due to the larger spatio-temporal concentration of weather extremes. Here we use the index of dispersion³⁸ to estimate temporal clustering for the whole simulation domain as well as regionally for Germany, the British Isles, and Alpine area. The domain-wide analysis is akin to estimating maximum simultaneous property losses, while the

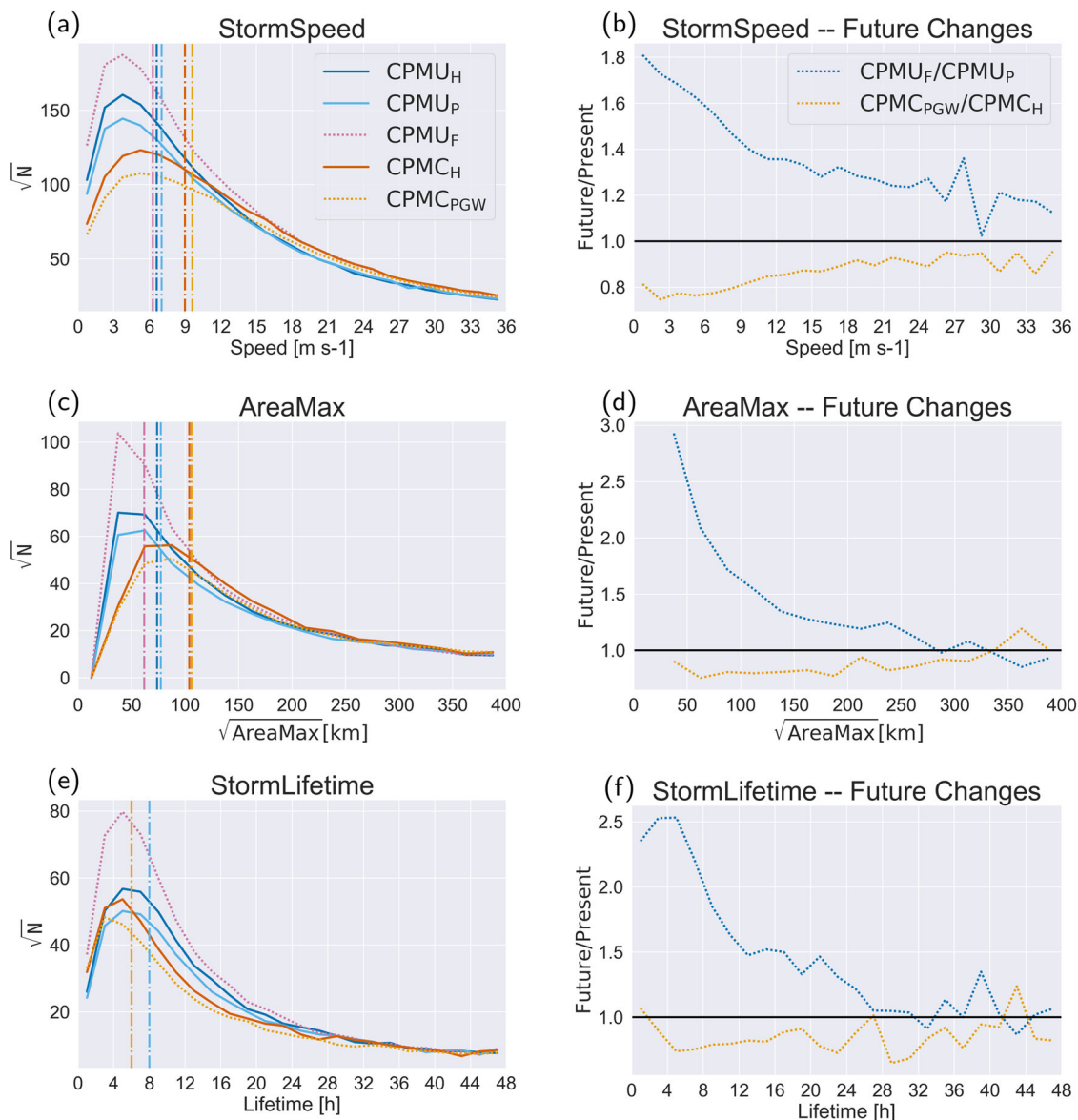


Fig. 4 Histograms of various storm properties and their future changes (continued). Similar to Fig. 3, but for **a, b** movement speed (StormSpeed), **c, d** maximum area (AreaMax), and **e, f** lifetime (StormLifetime). Vertical lines are used to indicate the median. All panels except **a** and **b** are diagnosed per MCS track. Storm speed in **a** and **b** is diagnosed hourly for each MCS.

regional analysis is focused on indicating the potential for compound hazards.

Table 2 presents the JJA and SON pentad index of dispersion ($\hat{\phi}$); we find clear evidence of temporal clustering of MCSs as all simulations have dispersion indices above 1 (indicating clustering). CPMC simulations show a lower level of clustering than the UKMO simulations. Europe-wide, both CPMs project MCS warm-season clustering to increase, but only SON increases are significant. For SON, dispersion indices increase from 25.5 (15.2) to 45.4 (24.4) for the UKMO UM (ETHZ COSMO) simulations, which are outside the confidence intervals of the timeslice estimates. However, JJA increases can be robust regionally (e.g. over Germany and the British Isles). There are no clear JJA changes for the Alpine region, although this region has large summer decreases to the precipitation mean and frequency^{19,39}, but a robust SON increase is found. For CPMU_F, SON shows large increases in precipitation extremes^{19,39}. The increase of MCS temporal clustering diagnosed here for both models will likely amplify the flood impacts of increases in precipitation volume

projected from the strongest MCSs. An alternate approach to assess clustering is by diagnosing the number of simultaneous objects-of-interest (i.e. MCSs) passing near a fixed point⁴⁰; this is examined in Supplementary Note 3, and results are consistent with the dispersion analysis here.

We now focus on identifying why the CPMs agree on projected increases in the total precipitation from MCSs, their contribution to the mean, and MCS peak intensity, whilst disagreeing on changes to the underlying number of MCSs and precipitation volume per individual storm. We start by considering storm speed and its relationship to storm area and lifetime. Movement speed and steering winds are closely linked to the vertical wind shear of the large-scale environment, which is crucial for the development and persistence of these deep convective storms (i.e. storm organisation)⁴¹, suggesting a movement speed (Fig. 4a, b) relationship with area and lifetime (Fig. 4c–f). Comparing the two hindcast simulations, storms are faster-moving and larger but more short-lived in the ETHZ simulations. Given the hindcasts have highly similar lateral boundary conditions (LBCs),

Table 2 The pentad index of dispersion (dimensionless, $\hat{\phi}$) for the number of MCSs.**Pentad MCS clustering by $\hat{\phi}$**

	Index of dispersion 5-dy pentad	
	<i>JJA Europe</i>	<i>JJA Alpine</i>
CPMU _H	29.9 (23.7, 35.1)	19.5 (13.0, 25.5)
CPMU _P	34.6 (23.5, 45.2)	25.4 (15.1, 36.4)
CPMU _F	35.2 (26.2, 43.9)	21.3 (15.0, 27.2)
CPMC _H	14.6 (11.8, 17.3)	8.6 (6.9, 10.1)
CPMC _{PGW}	17.1 (12.9, 21.3)	9.5 (7.4, 11.4)
	<i>SON Europe</i>	<i>SON Alpine</i>
CPMU _H	28.9 (24.0, 33.4)	15.9 (11.2, 21.0)
CPMU _P	25.5 (20.3, 30.2)	17.6 (12.7, 22.6)
CPMU _F	45.4 (36.0, 53.8)	23.8 (17.0, 30.7)
CPMC _H	15.2 (11.5, 18.8)	10.2 (7.7, 12.6)
CPMC _{PGW}	24.4 (16.7, 31.9)	13.8 (10.0, 17.2)
	<i>JJA Germany</i>	<i>JJA British Isles</i>
CPMU _H	9.4 (5.5, 14.9)	3.8 (2.6, 5.3)
CPMU _P	7.0 (5.0, 8.6)	4.6 (2.7, 6.3)
CPMU _F	13.9 (6.8, 22.9)	16.7 (7.9, 25.5)
CPMC _H	5.8 (4.7, 6.9)	2.9 (2.1, 3.6)
CPMC _{PGW}	8.0 (6.4, 9.5)	4.6 (2.6, 6.6)

The 95% CIs, estimated by pentad resampling, are shown in parentheses. Regions are defined in Supplementary Fig. 1.

differences in model numerics and physics appear to be a factor in determining MCS speed, but this is beyond the scope of this study (see “Methods” for LBC caveats and model differences).

In CPMU_F, we find that MCS speed decreases from 7.0 to 6.3 m s⁻¹³⁰ with maximum area and lifetime responding similarly (median $\sqrt{\text{AreaMax}}$: 77.3 → 61.9 km; median lifetime: 8 → 6 h). In contrast, CPMC_{PGW} projects somewhat faster (median speed: 9.0 → 9.6 m s⁻¹) and larger (median $\sqrt{\text{AreaMax}}$: 103.9 → 106.0 km) MCSs, resulting in a projected increase to average precipitation volume per MCS (panel e).

Robust aspects of MCS changes in both CPMs, including increases to total storm precipitation volume, peak storm intensities, and MCS temporal clustering, are important to climate impacts. Increases in peak precipitation intensities are well understood in terms of increases to saturation water vapour pressure with temperature²². However, CPMU_F and CPMC_{PGW} disagree on the magnitude of these changes. Changes to total storm volume, representing the combined effects of changes to the number of MCSs and precipitation volume per MCS, are driven by different underlying processes. In particular, precipitation volume per MCS is linked to storm movement speed (e.g., a proxy to vertical wind shear) which controls both convective organisation³ and the amount of time a storm precipitates over a catchment. CPMC_{PGW} indicates a different change in storm movement speed—faster MCSs—to the fully-dynamically downscaled CPMU_F simulation—storm slowdown. We note here that our results also suggest that different model physics may play a role in storm movement, as there are some differences between CPMU_H and CPMC_H hindcasts (Fig. 4). Model physics may also explain the differences in land-sea contrast in the spatial density of MCSs between the two models (Supplementary Note 2).

Our results highlight the importance of including circulation change uncertainties through sampling different driving GCMs and different downscaling approaches in projecting changes to MCS characteristics, particularly precipitation volume per MCS and number of MCSs, both critical for flood impacts. Additional experiments, for example a PGW-experiment with CPMU and standard GCM downscaling with CPMC, are needed to quantify the relative importance of the large-scale dynamics compared to

other factors (e.g. differences in model dynamics and physics) that may contribute to differences in different CPM projections. Nevertheless, large-scale circulation changes have been identified as a key driver of some aspects of MCS changes, e.g. storm movement speed³⁰. These large-scale changes may be different between CPMU_F and CPMC_{PGW} due to the different driving GCM and/or downscaling approach; we cannot disentangle these contributing factors with the experiments here. However, this study does identify the importance of large-scale circulation changes for impact-relevant changes in organised convective storms.

We expect the PGW approach to remain popular due to its lower computation cost and its advantage in constraining natural variability in climate change simulations. A standardisation of the PGW approach would be helpful; for instance, the PGW perturbations have been derived from multi-model means¹⁶ or a single GCM⁴². Initiatives like the recent Europe CPM collaboration³⁹ would help such a standardisation, with the broader goal of creating a favourable environment for climate model intercomparisons. We also recommend a coordinated set of GCM/PGW driven pairs are carried out, allowing a clear assessment of the importance of capturing changes in sub-seasonal circulation patterns for future changes in local climate extremes and limitations of the PGW approach. This will be valuable for informing future CPM experimental design.

Future large-scale circulation changes over Europe are uncertain^{28,29}, however, there is some consensus across models of a significant weakening of the summer circulation, with a shift of the polar jet and thus midlatitude cyclone tracks towards the north due to Arctic Amplification^{43,44}. This is manifested over Europe by CMIP simulations as reductions to synoptic variability^{29,43}. PGW approaches do not fully capture such changes, although new developments to PGW such as the one applied here²¹ do account for mean changes at synoptic time scales by superposing day-by-day annual cycle changes onto present-day variability. Since MCSs and other high-impact precipitation extremes are often triggered by synoptic variability (for example, changes to the frequency of cut-off lows that triggered the 2021 European floods⁴⁵), a multi-model downscaling of different GCMs is needed to assess uncertainty in the large-scale circulation change and to link these changes to organised convective storms. We therefore recommend that assessments of changes in convective storms must include a range of circulation change scenarios and downscaling approaches if possible. Given model physics and numerics are also important, a multi-model and/or parameter-perturbed ensemble of fully dynamically downscaled CPM future scenarios (like UKCP Local⁴⁶) would be recommended; this is not different to what the global climate modelling community has been doing^{47,48} but is a technical challenge at convection-permitting scales. The even longer-term goal is to achieve global climate CPM⁴⁹. Future work should also consider other (lower) emission scenarios, as RCP8.5, although plausible, is not the most likely scenario⁵⁰.

The significant increased contribution to European precipitation by intense, high-volume and clustered convective storms shown here has important social-economic implications, with (flash and fluvial) flooding, landslide and drought risks all expected to increase at the same time if hazard management remains as status-quo. Increased contributions to total precipitation from such storms under a drier European climate^{19,39} imply that water supply from precipitation will be distributed more unequally in space and time, increasing stresses to future water supply. Efforts to incorporate climate change into risk management approaches need to be fully embraced to ensure that robust climate adaptation measures are realised. It is important that results such as these are used to help society prepare for the impacts of more extreme future precipitation events.

Methods

Model simulations. The UKMO climate model simulations span Europe (Supplementary Fig. 1) at 2.2 km resolution^{11,19}. Three simulations with different LBCs are used: ERA-Interim⁵¹ driven and 25 km HadGEM3 present- and future-climate GCM driven simulations⁵². No intermediate nests are used. The model is based on the UKMO operational UKV model⁹. Cumulus parametrisation is disabled; a new semi-implicit semi-Lagrangian dynamical core and standard UKMO land-surface and boundary layer physics are used^{53–55}. Precipitation data are available hourly, and are regridded to 12 km grid boxes before carrying out any analysis.

The 10-year 25 km GCM present-climate simulation (CPMU_P) and ERA-Interim hindcast (CPMU_H) are for the period 1998–2007 and 1999–2008 respectively, and use daily observed SSTs⁵⁶. The future-climate end-of-century (2099–2108; CPMU_F) simulation uses the RCP8.5 greenhouse gas scenario²⁷. Future SSTs are observed SSTs plus 20-year mean changes that are derived from coupled GCM simulations⁵²; prescribed global mean SST change is $\approx 4\text{K}$ ⁵² but varies with time and regions.

The ETHZ COSMO CPM (aka COSMO-crCLIM) simulations^{20,57} have the same horizontal resolution and simulation domain. Different versions of COSMO are used in operational weather forecast and climate research across Europe²⁰. Unlike the UKMO simulations, the ETHZ simulations have a 12 km nested simulation⁵⁸ in between the driving data and the CPM. Substantial model physics differences exist between the ETHZ and UKMO simulations; for instance, the inclusion of a shallow-convection scheme in the ETHZ simulations⁵⁹, the use of a different land-surface and boundary layer scheme^{60,61}, and a split-explicit dynamical core for model numerics²⁰. There are two simulations: ERA-Interim⁵¹-driven hindcast (CPMC_H) and a PGW (CPMC_{PGW}) simulation²¹. Strictly speaking, due to the use of an intermediate nest, the ETHZ and UKMO hindcasts do not have the same LBCs; however, we expect the differences to be small away from the model lateral boundaries as the intermediate nest domain is not much larger than the CPM one⁵⁷. There are different flavours of the PGW approach, but they are all performed by adding some form of the global warming signal on top of reanalysis⁶². For the PGW simulation presented here, the seasonal cycle of changes to temperature, circulation, and stratification are first diagnosed from a specific CMIP5 RCP8.5 2070–2099 GCM simulation⁴², and are then superimposed onto 1999–2008 ERA-Interim data; this retains the multi-year mean seasonal changes but does not account for the changes to intra-seasonal and inter-annual circulation variability (i.e. the sequencing of weather events and the timing of NAOs are unchanged, etc.). Underlying global mean temperature change is $\approx 4\text{K}$ ⁴² but varies with time and regions. Like the UKMO data, data are available hourly, and are regridded to 12 km grid boxes.

RCP8.5 is a high emission scenario⁵⁰. Given CPMs are computationally expensive, RCP8.5 is often chosen to increase the robustness of the climate change response over natural variability.

All results are annual unless stated otherwise. The season of an individual MCS is determined by its initiation month. Only MCSs with their mean centroid location within the latitude-longitude box of [11°W – 25°E, 35.5°N – 59.5°N] are analysed.

DYMECS precipitation tracking algorithm. The precipitation system detection and tracking algorithm was originally developed for use with sub-hourly radar and forecast model precipitation data⁸. Since then, it has been applied to hourly climate model data over Africa with resolution as coarse as 25 km¹⁷.

The algorithm has two main parts: the detection of objects-of-interest for each image and the tracking of these objects-of-interest between consecutive images. The detection algorithm is based on the local table method⁶³: this is done by labelling pixels-of-interest (defined to be pixels with precipitation exceeding 1 mm/h) by line-by-line scanning. The tracking component is based on the windowed cross-correlation between consecutive images (hereby images at time $t - 1$ and t)⁶⁴. Each image is divided into 18-by-18 grid box windows with the centres of each window a half-window width apart. The correlations between each window at time $t - 1$ and t are computed. Velocities for a particular window are estimated using the distance to the window that has the maximum correlation with at time t . The labels that are identified at time $t - 1$ are then moved by those estimated velocities. Their areal overlap with labels at t are computed. If the overlap fraction exceeds 0.6, the overlapping labels are considered part of the same track, with splitting and merging allowed. A label with no valid predecessor is identified as a new track.

Definition of MCS. The definition here is inspired by previous work^{17,32}. We require MCSs to have maximum contiguous area of interest exceeding 1000 km², but they can have much greater maximum areas (100,000+ km²)³². Due to the relatively low precipitation threshold (1 mm h⁻¹) used to identify precipitation area, we only examine tracks with lifetime maximum intensity of at least 20 mm h⁻¹, thereby removing weaker precipitation tracks from the analysis.

In the 10-year hindcast and present-climate UKMO simulation data, there are ≈ 1183 and ≈ 860 tracks per April–September (AMJJAS) annually that satisfy the above criteria. Similarly, the 10-year ETHZ hindcast has ≈ 1184 tracks per AMJJAS. This is comparable to the number of tracks identified with outgoing longwave radiation (OLR) over a similar European domain for the same months³²—6311 tracks in five AMJJAS seasons (1993–1997; i.e. ≈ 1262 tracks per AMJJAS). However, we note an OLR-only analysis has severe limitations⁵. This is

further explored in Supplementary Note 4, where we show model OLR can falsely indicate areas of precipitation. Comparisons of the spatial pattern for AMJJAS are in Supplementary Note 2 as part of the discussion showing the land-sea differences between the two models.

Precipitation volume. The time-integrated precipitation volume from track i is its areal sum over all times:

$$\text{PrVol}_i = \sum_{\text{life}=1}^{\text{life}_i} \text{MeanPr}_{i,t} \times A_{i,t} \quad (1)$$

The PrVol_i has units of volume L^3 . The total volume follows naturally as:

$$\mathbf{V} = \sum_{i=1}^{n\text{Tracks}} \text{PrVol}_i \quad (2)$$

Total precipitation volume, from MCSs and non-MCSs, is calculated by spatially summing precipitation, either annually or seasonally, across the entire model simulation MCS domain. Annual (seasonal) totals only compare with annual (seasonal) MCS totals.

Temporal clustering. Temporal clustering of MCS is examined using count data statistics. Count clustering is measured by the index of dispersion $\hat{\phi}$ ³⁸, which is the quotient between the variance $\sigma_{n\text{MCS}}^2$ and the mean ($E(n\text{MCS})$):

$$\hat{\phi} = \frac{\sigma_{n\text{MCS}}^2}{E(n\text{MCS})} \quad (3)$$

$\hat{\phi} \approx 1$ if counts are randomly distributed (i.e. a Poisson Process); values much greater than 1.0 suggest temporal clustering. The above is calculated by aggregating daily counts into pentad (5-day) sums; weather systems generally persist for a few days, and the 5-day aggregation reduces serial correlation between the intervals. We examine the pentad index of dispersion in JJA and SON, accounting for the seasonal cycle and the higher frequency of MCSs during the warm season. Confidence intervals are estimated by recomputing the index 10,000 times by pentad bootstrapping (see “Bootstrapping method” for details).

Bootstrapping method. Confidence intervals are estimated by block bootstrapping data, assuming independence between blocks (pentad or year). Blocks are resampled with replacement, with the same sample size as in the original data, and the metric of interest is recomputed. This process is repeated, generating new estimates to the same metric. The 95 percentile interval is estimated by taking the 2.5 and 97.5 percentile of the bootstrap.

Regional analysis. The clustering index and certain precipitation indices are calculated regionally—British Isles (an ex-Mediterranean maritime region), Germany (an ex-Mediterranean continental region), and the CORDEX Alpine domain which is subject to multi-CPM study^{39,65}. The “Alpine” region covers central and southern Europe, including Switzerland, Austria, southern France and Germany, northern Italy, Adriatic Sea, Ligurian Sea, and the Gulf of Genoa; for this region, heavy precipitation is common for both summer over land and autumn over sea. The regions are illustrated in Supplementary Fig. 1. Finally, we note that temporal clustering and impacts occur at even smaller scales (river catchment or a city), but changes at that these scales are hard to diagnose with just 10-year climate simulations.

Data availability

The MCS-tracked data produced and analysed in this study are available from the UK Centre for Environmental Data Analysis⁶⁶. For the GPM-IMERG analysis in the Supplementary Information, the data can be openly accessed from Globus⁶⁷ under this link—https://app.globus.org/file-manager?origin_id=8cd89322-239f-49e1-bd6a-11923e335180&origin_path=%2F. Due to the high data volume, the raw climate model data are not publicly available. The Met Office model data used are under Crown copyright of the UK government, and access may be requested from the Met Office. The ETHZ model data are available upon reasonable request from ETH-Zurich. A subset of the raw model data will be made publicly available in the future through the Earth System Grid Federation nodes with other CORDEX-style simulations.

Code availability

Python and R code examples in how to read the MCS-tracked data are included in the metadata of the CEDA-uploaded data⁶⁶. Post-tracking analysis and generated figures are based on open-source Python packages, including cartopy version 0.20.3⁶⁸, matplotlib version 3.5.2⁶⁹, pandas versions 1.1.5 and 1.4.3⁷⁰, and seaborn version 0.11.2⁷¹, which are covered under the GNU (Lesser) General Public License. Cartopy uses resources from Natural Earth, which requires no citation nor permission to use. The source code for the tracking scheme is available on GitHub with public release version 1.0.0⁷².

Received: 26 May 2022; Accepted: 21 December 2022;

Published online: 05 January 2023

References

- Doswell, C. A., Brooks, H. E. & Maddox, R. A. Flash flood forecasting: an ingredients-based methodology. *Weather Forecast.* **11**, 560–581 (1996).
- Markowski, P. & Richardson, Y. Mesoscale convective systems. In *Mesoscale Meteorology in Midlatitudes*, 245–272 (John Wiley & Sons, Ltd, 2010). <https://onlinelibrary.wiley.com/doi/book/10.1002/9780470682104>.
- Schumacher, R. S. & Rasmussen, K. L. The formation, character and changing nature of mesoscale convective systems. *Nat. Rev. Earth Environ.* **1**, 300–314 (2020).
- Morel, C. & Senesi, S. A climatology of mesoscale convective systems over Europe using satellite infrared imagery. I: methodology. *Q. J. R. Meteorol. Soc.* **128**, 1953–1971 (2002).
- Feng, Z. et al. A global high-resolution mesoscale convective system database using satellite-derived cloud tops, surface precipitation, and tracking. *J. Geophys. Res. Atmos.* **126**, e2020JD034202 (2021).
- Yang, Q., Houze Jr., R. A., Leung, L. R. & Feng, Z. Environments of long-lived mesoscale convective systems over the central United States in convection permitting climate simulations. *J. Geophys. Res. Atmos.* **122**, 13,288–13,307 (2017).
- Higgins, R. W., Yao, Y., Yarosh, E. S., Janowiak, J. E. & Mo, K. C. Influence of the great plains low-level jet on summertime precipitation and moisture transport over the central United States. *J. Clim.* **10**, 481–507 (1997).
- Stein, T. H. M. et al. The three-dimensional morphology of simulated and observed convective storms over Southern England. *Mon. Weather Rev.* **142**, 3264–3283 (2014).
- Roberts, N. M. & Lean, H. W. Scale-selective verification of rainfall accumulations from high-resolution forecasts of convective events. *Mon. Weather Rev.* **136**, 78–97 (2008).
- Kendon, E. J., Roberts, N. M., Senior, C. A. & Roberts, M. J. Realism of rainfall in a very high resolution regional climate model. *J. Clim.* **25**, 5791–5806 (2012).
- Berthou, S. et al. Pan-European climate at convection-permitting scale: a model intercomparison study. *Clim. Dyn.* **55**, 35–59 (2020).
- Fumière, Q. et al. Extreme rainfall in Mediterranean France during the fall: added value of the CNRM-AROME Convection-Permitting Regional Climate Model. *Clim. Dyn.* **55**, 77–91 (2020).
- Luu, L. N., Vautard, R., Yiou, P. & Soueyroux, J.-M. Evaluation of convection-permitting extreme precipitation simulations for the south of France. *Earth Syst. Dyn. Discuss.* **2020**, 1–24 (2020).
- Caillaud, C. et al. Modelling Mediterranean heavy precipitation events at climate scale: an object-oriented evaluation of the CNRM-AROME convection-permitting regional climate model. *Clim. Dyn.* <https://doi.org/10.1007/s00382-020-05558-y> (2021).
- Thomassen, E. D. et al. Differences in representation of extreme precipitation events in two high resolution models. *Clim. Dyn.* <https://link.springer.com/article/10.1007/s00382-021-05854-1> (2021).
- Prein, A. F. et al. Simulating North American mesoscale convective systems with a convection-permitting climate model. *Clim. Dyn.* **55**, 1–16 (2017).
- Crook, J. et al. Assessment of the representation of West African storm lifecycles in convection-permitting simulations. *Earth Space Sci.* **6**, 818–835 (2019).
- Hentgen, L., Ban, N., Kröner, N., Leutwyler, D. & Schär, C. Clouds in convection-resolving climate simulations over Europe. *J. Geophys. Res. Atmos.* **124**, 3849–3870 (2019).
- Chan, S. C. et al. Europe-wide precipitation projections at convection permitting scale with the unified model. *Clim. Dyn.* **55**, 409–428 (2020).
- Schär, C. et al. Kilometer-scale climate models: prospects and challenges. *Bull. Am. Meteorol. Soc.* **101**, E567–E587 (2020).
- Brogli, R., Heim, C., Sørland, S. L. & Schär, C. The pseudo-global-warming (PGW) approach: methodology, software package PGW4ERA5 v1.1, validation and sensitivity analyses. *Geosci. Model Dev. Discuss.* **2022**, 1–28 (2022).
- Trenberth, K. E., Dai, A., Rasmussen, R. M. & Parsons, D. B. The changing character of precipitation. *Bull. Am. Meteorol. Soc.* **84**, 1205–1217 (2003).
- Prein, A. F. et al. Increased rainfall volume from future convective storms in the US. *Nat. Clim. Change* **7**, 880–884 (2017).
- Fowler, H. J. et al. Towards advancing scientific knowledge of climate change impacts on short-duration rainfall extremes. *Philos. Trans. R. Soc. A Math. Phys. Eng. Sci.* **379**, 20190542 (2021).
- Schiemann, R. et al. The resolution sensitivity of northern hemisphere blocking in four 25-km atmospheric global circulation models. *J. Clim.* **30**, 337–358 (2017).
- Moreno-Chamarro, E. et al. Impact of increased resolution on long-standing biases in highresmp-primavera climate models. *Geosci. Model Dev.* **15**, 269–289 (2022).
- Meinshausen, M. et al. The RCP greenhouse gas concentrations and their extensions from 1765 to 2300. *Clim. Change* **109**, 213–241 (2011).
- Zappa, G., Shaffrey, L. C., Hodges, K. I., Sansom, P. G. & Stephenson, D. B. A multimodel assessment of future projections of North Atlantic and European extratropical cyclones in the CMIP5 climate models*. *J. Clim.* **26**, 5846–5862 (2013).
- Harvey, B. J., Cook, P., Shaffrey, L. C. & Schiemann, R. The response of the northern hemisphere storm tracks and jet streams to climate change in the CMIP3, CMIP5, and CMIP6 climate models. *J. Geophys. Res. Atmos.* **125**, e2020JD032701 (2020).
- Kahraman, A., Kendon, E. J., Chan, S. C. & Fowler, H. Quasi-stationary intense rainstorms spread across europe under climate change. *Geophys. Res. Lett.* <https://doi.org/10.1029/2020GL092361> (2021).
- Tuduri, E. & Ramis, C. The environments of significant convective events in the Western Mediterranean. *Weather Forecast.* **12**, 294–306 (1997).
- Morel, C. & Senesi, S. A climatology of mesoscale convective systems over europe using satellite infrared imagery. II: characteristics of european mesoscale convective systems. *Q. J. R. Meteorol. Soc.* **128**, 1973–1995 (2002).
- Hu, H., Feng, Z. & Leung, L.-Y. R. Linking flood frequency with mesoscale convective systems in the US. *Geophys. Res. Lett.* **48**, e2021GL092546 (2021).
- Kendon, E. J. et al. Heavier summer downpours with climate change revealed by weather forecast resolution model. *Nat. Clim. Change* **4**, 570–576 (2014).
- Ban, N., Schmidli, J. & Schär, C. Heavy precipitation in a changing climate: does short-term summer precipitation increase faster? *Geophys. Res. Lett.* **42**, 1165–1172 (2015).
- Prein, A. F. et al. The future intensification of hourly precipitation extremes. *Nat. Clim. Change* **7**, 48–52 (2017).
- Pucik, T. et al. Future changes in European severe convection environments in a regional climate model ensemble. *J. Clim.* **30**, 6771–6794 (2017).
- Mailier, P. J., Stephenson, D. B., Ferro, C. A. T. & Hodges, K. I. Serial clustering of extratropical cyclones. *Mon. Weather Rev.* **134**, 2224–2240 (2006).
- Pichelli, E. et al. The first multi-model ensemble of regional climate simulations at kilometer-scale resolution part 2: historical and future simulations of precipitation. *Clim. Dyn.* <https://doi.org/10.1007/s00382-021-05657-4> (2021).
- Bevacqua, E., Zappa, G. & Shepherd, T. G. Shorter cyclone clusters modulate changes in European wintertime precipitation extremes. *Environ. Res. Lett.* **15**, 124005 (2020).
- Weisman, M. L. & Klemp, J. B. The dependence of numerically simulated convective storms on vertical wind shear and buoyancy. *Mon. Weather Rev.* **110**, 504–520 (1982).
- Kroener, N. et al. Separating climate change signals into thermodynamic, lapse-rate and circulation effects: theory and application to the European summer climate. *Clim. Dyn.* **48**, 3425–3440 (2017).
- Coumou, D., Lehmann, J. & Beckmann, J. The weakening summer circulation in the Northern Hemisphere mid-latitudes. *Science* **348**, 324–327 (2015).
- Smith, D. M. et al. The polar amplification model intercomparison project (PAMIP): contribution to CMIP6: investigating the causes and consequences of polar amplification. *Geosci. Model Dev.* **12**, 1139–1164 (2019).
- Kreienkamp, F. et al. Rapid attribution of heavy rainfall events leading to the severe flooding in western Europe during July 2021 (2021).
- Kendon, E. J. et al. *Update to UKCP local (2.2km) Projections*. Tech. Rep. (United Kingdom Met Office, 2021). <https://www.metoffice.gov.uk/research/approach/collaboration/ukcp/guidance-science-reports>.
- Murphy, J. M. et al. Quantification of modelling uncertainties in a large ensemble of climate change simulations. *Nature* **430**, 768–772 (2004).
- Eyring, V. et al. Overview of the coupled model intercomparison project phase 6 (CMIP6) experimental design and organisation. *Geosci. Model Dev.* **8**, 10539–10583 (2016).
- Stevens, B. et al. DYAMOND: the DYNAMics of the Atmospheric general circulation Modeled On Non-hydrostatic Domains. *Prog. Earth Planet. Sci.* **6**, 61 (2019).
- Hausfather, Z. & Peters, G. P. Emissions—the ‘business as usual’ story is misleading. <https://www.nature.com/articles/d41586-020-00177-3> (2020).
- Dee, D. P. et al. The ERA-interim reanalysis: configuration and performance of the data assimilation system. *Q. J. R. Meteorol. Soc.* **137**, 553–597 (2011).
- Mizielinski, M. S. et al. High resolution global climate modelling: the UPSCALE project, a large simulation campaign. *Geosci. Model Dev.* **7**, 1629–1640 (2014).
- Boutle, I. A., Eyre, J. E. J. & Lock, A. P. Seamless stratocumulus simulation across the turbulent gray zone. *Mon. Weather Rev.* **142**, 1655–1668 (2014).
- Best, M. J. et al. The Joint UK Land Environment Simulator (JULES), model description—part 1: energy and water fluxes. *Geosci. Model Dev.* **4**, 677–699 (2011).

55. Wood, N. et al. An inherently mass-conserving semi-implicit semi-Lagrangian discretisation of the deep-atmosphere global nonhydrostatic equations. *Q. J. R. Meteorol. Soc.* **140**, 1505–1520 (2014).
56. Donlon, C. et al. The Operational Sea Surface Temperature and Sea Ice Analysis (OSTIA) system. *Remote Sens. Environ.* **116**, 140–158 (2012).
57. Leutwyler, D., Lüthi, D., Ban, N., Fuhrer, O. & Schär, C. Evaluation of the convection-resolving climate modeling approach on continental scales. *J. Geophys. Res.* **122**, 5237–5258 (2017).
58. Kotlarski, S. et al. Regional climate modeling on European scales: a joint standard evaluation of the EURO-CORDEX RCM ensemble. *Geosci. Model Dev.* **7**, 1297–1333 (2014).
59. Theunert, F. & Seifert, A. Simulation studies of shallow convection with the convection-resolving version of DWD Lokal-Modell. *COSMO Newsletter* **6**, 121–128 (2006).
60. Mellor, G. L. & Yamada, T. Development of a turbulence closure model for geophysical fluid problems. *Rev. Geophys.* **20**, 851–875 (1982).
61. Heise, E., Ritter, B. & Schrodin, R. *COSMO Tech. Rep., No. 9: Operational Implementation of the Multilayer Soil Model*. Tech. Rep. (Deutscher Wetterdienst, 2006). <https://www.cosmo-model.org/content/model/documentation/techReports/cosmo/default.htm>.
62. Schär, C., Frei, C., Lüthi, D. & Davies, H. C. Surrogate climate change scenarios for regional climate models. *Geophys. Res. Lett.* **23**, 669–672 (1996).
63. Haralick, R. M. & Shapiro, L. G. *Computer and Robot Vision* 1st edn (Addison-Wesley Longman Publishing Co., Inc., 1992).
64. Rinehart, R. E. & Garvey, E. T. Three-dimensional storm motion detection by conventional weather radar. *Nature* **273**, 287–289 (1978).
65. Ban, N. et al. The first multi-model ensemble of regional climate simulations at kilometer-scale resolution, part I: evaluation of precipitation. *Clim. Dyn.* <https://doi.org/10.1007/s00382-021-05708-w> (2021).
66. Chan, S. C. et al. Mesoscale convective system tracks, diagnosed from European 2.2km climate model simulations. <https://doi.org/10.5285/f39f0aa295304d55beeb0a850760b061> (2022).
67. Allen, B. et al. Software as a service for data scientists. *Commun. ACM* **55**, 81–88 (2012).
68. Met Office. *Cartopy: A Cartographic Python Library with a Matplotlib Interface* (Exeter, Devon, 2010–2015). <https://scitools.org.uk/cartopy>.
69. Hunter, J. D. Matplotlib: a 2D graphics environment. *Comput. Sci. Eng.* **9**, 90–95 (2007).
70. Pandas Development Team. T. pandas-dev/pandas: Pandas. <https://doi.org/10.5281/zenodo.3509134> (2020).
71. Waskom, M. L. Seaborn: statistical data visualization. *J. Open Source Softw.* **6**, 3021 (2021).
72. Chan, S. & Crook, J. DYMECS Tracking for climate model data, OCTAVE-version 1.0.0. <https://doi.org/10.5281/zenodo.7376727> (2022).
73. Delrieu, G. et al. The catastrophic flash-flood event of 8–9 september 2002 in the Gard region, France: a first case study for the Cévennes-Vivarais Mediterranean Hydrometeorological Observatory. *J. Hydrometeorol.* **6**, 34–52 (2005).
74. Mathias, L., Ermert, V., Kelemen, F. D., Ludwig, P. & Pinto, J. G. Synoptic analysis and hindcast of an intense bow echo in Western Europe: the 9 June 2014 storm. *Weather Forecast.* **32**, 1121–1141 (2017).
75. Součková, M. & Doležal, J. *Zpráva k vyhodnocení tornáda na jihu Moravy 24. 6. 2021 Meteorologické zhodnocení*. Tech. Rep. (Czech Hydrometeorological Institute, 2021). https://www.chmi.cz/files/portal/docs/tiskove_zpravy/2021/Zprava_k_tornadu_1.pdf.
76. Carr, D. B., Littlefield, R. J., Nicholson, W. L. & Littlefield, J. S. Scatterplot matrix techniques for large N. *J. Am. Stat. Assoc.* **82**, 424–436 (1987).

Acknowledgements

We would like to acknowledge the following persons (ordered by surname) for their support in this work: Ségolène Berthou (Met Office Hadley Centre), Demory Marie-Estelle (ETH-Zürich), Christoph Schär (ETH-Zürich), Emma D Thomassen (Technical University of Denmark, Danish Meteorological Institute), and Jesús Vergara Temprado

(UBS Group AG, ETH-Zürich). This research is supported by the United Kingdom NERC Changing Water Cycle programme (FUTURE-STORMS; grant: NE/R01079X/1), European Union Horizon 2020 (European Climate Prediction System (EUCP) project; grant: 776613), and European Research Council (INTENSE; grant: ERC-2013-CoG-617329). E.J.K. also gratefully acknowledges funding from the Joint UK BEIS/Defra Met Office Hadley Centre Climate Programme (GA01101). H.J.F. is a Royal Society Wolfson Research Merit Award (WM140025) holder. ETH Zürich and Universität Innsbruck acknowledge the Partnership for advanced computing in Europe (PRACE) for awarding access to Piz Daint at ETH Zürich/Swiss National Supercomputing Center (Switzerland) for conducting COSMO simulations, and Helmholtz Data Federation initiative for Jülich Supercomputing Centre (Germany) providing necessary data exchange infrastructure and services. COSMO-crCLIM was developed in collaboration with the Federal Office for Meteorology and Climatology MeteoSwiss, the Swiss National Supercomputing Centre (CSCS) and the Center for Climate Systems Modeling (C2SM) at ETH Zürich. Free-and-open-source software Python, R, GNU Octave are used in the analysis. Finally, we would like to thank the anonymous reviewers of this manuscript.

Author contributions

S.C.C. co-wrote the manuscript, conducted data analysis and data visualisation. E.J.K. co-wrote the manuscript, supplied the data, performed the UKMO model simulations. H.J.F. advised on the analysis methodologies, discussed the results, co-wrote and commented on the manuscript. A.K. conducted data analysis and advised on analysis methodologies. J.C. provided the necessary software code for the analysis. N.B. provided ETH-Zürich data for analysis, performed the ETHZ simulations, and commented on the manuscript. A.F.P. conducted data analysis, and co-wrote and commented on the manuscript.

Competing interests

The authors declare no competing interests.

Additional information

Supplementary information The online version contains supplementary material available at <https://doi.org/10.1038/s43247-022-00669-2>.

Correspondence and requests for materials should be addressed to Steven C. Chan.

Peer review information *Communications Earth & Environment* thanks Jakob Zscheischler and the other, anonymous, reviewer(s) for their contribution to the peer review of this work. Primary Handling Editors: Clare Davis, Heike Langenberg. Peer reviewer reports are available.

Reprints and permission information is available at <http://www.nature.com/reprints>

Publisher's note Springer Nature remains neutral with regard to jurisdictional claims in published maps and institutional affiliations.



Open Access This article is licensed under a Creative Commons Attribution 4.0 International License, which permits use, sharing, adaptation, distribution and reproduction in any medium or format, as long as you give appropriate credit to the original author(s) and the source, provide a link to the Creative Commons license, and indicate if changes were made. The images or other third party material in this article are included in the article's Creative Commons license, unless indicated otherwise in a credit line to the material. If material is not included in the article's Creative Commons license and your intended use is not permitted by statutory regulation or exceeds the permitted use, you will need to obtain permission directly from the copyright holder. To view a copy of this license, visit <http://creativecommons.org/licenses/by/4.0/>.

© The Author(s) 2023